

The Retrocalcarine Sulcus Is Functionally Distinct Between Macaques and Humans

Michael Arcaro (✉ marcaro@sas.upenn.edu)

University of Pennsylvania <https://orcid.org/0000-0002-4612-9921>

Margaret S. Livingstone

Harvard Medical School

Kendrick N. Kay

University of Minnesota Twin Cities: University of Minnesota Twin Cities

Kevin S. Weiner

University of California Berkeley

Research Article

Keywords: vision, comparative neuroanatomy, striate cortex, calcarine sulcus, human, macaque

DOI: <https://doi.org/10.21203/rs.3.rs-529574/v1>

License: © ⓘ This work is licensed under a Creative Commons Attribution 4.0 International License.

[Read Full License](#)

The retrocalcarine sulcus is functionally distinct between macaques and humans

Michael J. Arcaro¹, Margaret S. Livingstone², Kendrick N. Kay³, Kevin S. Weiner^{4,5}

¹ Department of Psychology, University of Pennsylvania, Philadelphia, PA 19146

² Department of Neurobiology, Harvard Medical School, Boston, MA, 02115

³ Center for Magnetic Resonance Research (CMRR), Department of Radiology, University of Minnesota, Minneapolis, MN, 55455

⁴ Department of Psychology, University of California, Berkeley, Berkeley, CA 94720

⁵ Helen Wills Neuroscience Institute, University of California, Berkeley, Berkeley, CA 94720

Corresponding Author:

Kevin S. Weiner, Department of Psychology, University of California, Berkeley, Berkeley, CA 94720, kweiner@berkeley.edu

ABSTRACT

Primate cerebral cortex is highly convoluted with much of the cortical surface buried in sulcal folds. The origins of cortical folding and its functional relevance has been a major focus of systems and cognitive neuroscience. Stereotyped patterns of cortical folding across individuals and multiple primate species indicate common evolutionary pressures in their development. However, foundational questions regarding organizing principles shared across species remain unanswered. Taking a cross-species comparative approach with a careful consideration of historical observations, we investigate cortical folding within the calcarine sulcus, a primary fold in primates. We identify two macroanatomical structures – the retrocalcarine and external calcarine sulci – in 24 humans and 6 macaque monkeys. We show that within species, these sulci are identifiable in all individuals, fall on a similar part of the V1 retinotopic map, and thus, serve as anatomical landmarks predictive of functional organization. Yet, across species, the actual underlying visual field representations differ strikingly across humans and macaques. Thus, the structure-function correspondence for an evolutionarily old structure like V1 is species-specific and suggests intriguing differences in developmental constraints across primates.

Keywords: vision, comparative neuroanatomy, striate cortex, calcarine sulcus, human, macaque

Declarations:

Funding: This research was supported by Start-up funds provided by UC Berkeley (to KSW) and by R01EY16187 and P30EY012196 (to MSL).

Conflicts of interest: None

Availability of data and material: Data will be made available from the first author upon request.

Authors' contributions: Conceptualization, K.N.K. and K.S.W., Methodology, M.J.A., K.N.K., and K.S.W., Investigation, M.J.A., K.N.K., and K.S.W., Writing, M.J.A., K.N.K., and K.S.W.

Ethics approval: All procedures were approved by the Harvard Medical School Animal Care and Use Committee and conformed with National Institutes of Health guidelines for the humane care and use of laboratory animals.

Consent to participate: N/A

Consent for publication: All authors consent

INTRODUCTION

A major goal in systems and cognitive neuroscience is to understand the evolution of the human cerebral cortex (Van Essen 2007; Zilles et al. 2013). A central focus of this goal is to examine and quantify the correspondence between sulcal or gyral features relative to architectonically or functionally defined maps across different primate species (Van Essen 2007). Despite the widespread interest and a general convergence of conclusions across studies regarding comparisons of primary structures (e.g. the calcarine sulcus, CaS) and primary sensory areas (e.g. visual area V1; for reviews, see Rosa and Tweedale 2005; Van Essen 2007; Zilles et al. 2013; Arcaro and Kastner 2015; Van Essen et al. 2018; Van Essen and Glasser 2018), foundational questions still remain unexplored largely because several historical observations have been commonly overlooked, which in turn, has generated modern discrepancies. Resolving these discrepancies through focused, cross-species comparative studies is critically necessary in order to produce accurate insights regarding the evolution of the cerebral cortex. As a majority (nearly 60-70%; Armstrong et al. 1995; Van Essen 2007; Van Essen et al. 2018) of the human cerebral cortex is buried in sulci, accurate insights regarding the coupling (or not) between sulci and functional maps are especially crucial.

For example, in the very first labeling of the CaS in 1861, Huxley described a bifurcation in the posterior CaS in human¹ and *Ateles* (spider monkey)² (Figure 1A; Huxley 1861). Furthermore, in the late 19th and early 20th centuries, this portion of the CaS was so frequently identified across species (Figure 1) and was found to appear differentially in gestation compared to the CaS proper, that anatomists argued over distinct names for this vertical component of the CaS. For example, Cunningham (1892) referred to it eponymically as the vertical fissure of Sietz (1886)³ as well as the posterior calcarine sulcus (Cunningham 1892), while Smith suggested the term retrocalcarine (rCaS) sulcus (Smith 1903).⁴ Despite historical interest and contentions regarding this sulcus, there is still modern discrepancy regarding the existence of this bifurcation in humans. For example, while Iaria and colleagues (Iaria and Petrides 2007; Iaria et al. 2008) identified and quantified the morphological features of the rCaS in living and post-mortem

¹Huxley writes: “Traced from before backwards, or from within outwards, the line of this sulcus presents a strongly marked, but irregular, upward convexity. On making successive transverse sections of this cerebrum from before backwards (woodcut, fig. 1. A, B, C, D), the fissure was seen, in its most posterior part (A), to pass almost horizontally outwards for a short distance, and then to divide into an upward and a downward branch.”

² Huxley writes: “The calcarine sulcus, I, I, has the same general direction and the same bifurcated termination, as in Man.”

³ In the original paper, Sietz (1886) referred to this sulcus as “Endfurche, F. extrema” ((Sietz 1886), pg. 275). See Supplementary Figure 1 for images from Sietz (1886).

⁴ Smith (Smith 1904a) credits Cunningham as the “first writer to draw any distinction between the calcarine and the retrocalcarine sulci. His reason for doing so was, briefly, the fact that the latter sulcus developed later and independently of the calcarine” (Smith 1904a, pg.128). Cunningham, however, did not use the retrocalcarine nomenclature. He referred to this sulcus as *fissure calcarina posterior*. Smith (1903) proposed the retrocalcarine name: “The sulcus which Cunningham calls “posterior calcarine” develops later and quite independently of the anterior sulcus; it never becomes as deep as the former; as a rule it does not share in the formation of the calcar, and in many cases it is separated from the anterior or calcarine sulcus by a submerged fold of cortex. It is, to use Cunningham’s own words, “a *secondary sulcus* in every sense of the term.” It is therefore of a very different nature to the true calcarine sulcus, and, as it is convenient to have a distinctive name, I shall call it “retrocalcarine,” because it is placed on the caudal side of the calcar... This has been done, not for pedantic reasons, but because a separate name becomes absolutely necessary in Comparative Anatomy, where the fundamental distinction between the two elements becomes more pronounced” (Smith 1903) pg. 386).

participants, Van Essen (2007), in the same year, stated that humans do not have this bifurcated sulcus:

"The calcarine sulcus also varies in shape, having a characteristic T-shaped posterior bifurcation in the macaque and chimpanzee that is lacking in humans." (Van Essen, 2007, pg. 271)

[Figure 1 Here]

We speculate that a main reason that cortical cartographers may not clearly identify the rCaS in humans is due to the way in which functional areas are typically defined *in vivo* using functional magnetic resonance imaging (fMRI). Common approaches for functional mapping of the human brain such as inflating or flattening a digitally reconstructed cortical surface provide utility by visualizing areas buried within sulci, which comprise the majority of cortex. However, the inflation and flattening process invariably distorts important features of the cortex. For example, while the rCaS is easily identifiable in post-mortem brains (Figure 1A) as well as the wrinkled (or pial) versions of cortical surface reconstructions, the inflation and flattening process can visually distort the rCaS to the point that it is not differentiable from the horizontal portion of the calcarine (Figure 2).

[Figure 2 Here]

Taking these methodological concerns into consideration, the present study compares eccentricity measurements in the rCaS and the nearby external calcarine sulci (eCaS) using fMRI in human participants (N=24) and macaques (N=6). We focused on eccentricity representations as classic electrophysiology studies have related eccentricity representations to the rCaS in macaques (Van Essen et al. 1984; Horton and Hocking 1996). Despite similarities in morphology between the two species, the macaque rCaS comprises retinotopic representations 2-3 times further in the periphery than the human rCaS. In both species, the eCaS comprises retinotopic representations of central visual space with representations closer to the fovea in the humans. We discuss these findings in the context of understanding how the same macroanatomical structure across species could evolve different functional representations, as well as how functionally homologous areas across species can have different underlying anatomical substrates.

MATERIALS AND METHODS

Participants.

Humans. Twenty-four adults (ages 22-35, 14 female) were randomly selected from the 181 participants comprising the HCP 7T Retinotopy Dataset (HCP7TRET; Benson et al. 2018). All participants had normal or corrected-to-normal visual acuity. Each participant was assigned a six-digit HCP ID.

Macaques. Six juvenile *Macaca mulattas* (3 female) participated in this study. Four monkeys were selected from (Arcaro et al. 2017). All procedures were approved by the Harvard Medical School Animal Care and Use Committee and conformed with National Institutes of Health guidelines for the humane care and use of laboratory animals. For scanning, monkeys were alert and their heads were immobilized using a foam-padded helmet with a chinstrap that delivered juice. The monkeys were scanned in a primate chair that allowed them to move their bodies and limbs freely, but their heads were restrained in a forward-looking position by the padded helmet.

Stimuli. For both human and macaque experiments, visual stimuli were projected onto a screen at the end of the scanner bore.

Human retinotopic mapping. In the HCP7RET experiment, retinotopic mapping stimuli were constructed by creating slowly moving apertures consisting of rotating wedges, expanding/contracting annuli, and oriented bars constrained to a circular region with a diameter of 16° centrally presented on the screen. Dynamic colorful textures composed of objects on an achromatic pink-noise background were placed within the apertures. Apertures were animated at 15 Hz. Each run lasted 300 s with a total of 6 runs per participant. Participants were instructed to maintain fixation on a centrally presented dot and to perform a color change detection task. See Benson et al. 2018 for more details.

Macaque retinotopic mapping. Retinotopic mapping stimuli were constructed by creating slowly moving apertures consisting of rotating wedges and expanding/contracting annuli constrained to a circular region with a diameter of 20° centrally presented on the screen. Dynamic colorful checkerboards filled the apertures in which each check's chromaticity and luminance alternated at the flicker frequency of 4 Hz. Polar angle (wedge) and eccentricity (annulus) mapping were conducted in separate experiments each consisting of 8-12 runs with an equal split in the direction of rotation. Each polar angle run consisted of eight cycles lasting 40 s each. Each eccentricity run consisted of seven cycles lasting 40 s each with 10 s of blank, as well as black backgrounds in between. These additional blank periods were inserted to temporally separate responses to the foveal and most peripheral positions. The monkeys were rewarded with juice for maintaining a central fixation within a 2° window. Gaze direction was monitored using an infrared eye tracker (ISCAN, Burlington, MA). See Arcaro et al. 2017 for more details.

Data acquisition. Human data were collected at the Center for Magnetic Resonance Research at the University of Minnesota using a Siemens 7T Magnetom actively shielded scanner and a 32-channel received coil array with a single channel transmit coil (Nova Medical, Wilmington, MA). Macaque functional data were collected in a 3T Siemens TimTrio scanner with an AC88 gradient insert using 4-channel surface coils (custom made by Azma Maryam at the Martinos

Imaging Center). Macaque anatomical data were collected in a 3T Siemens Skyra scanner using a 16-channel coil.

Human anatomical scans. T1-weighted (T1w) and T2-weighted (T2w) structural scans at 0.7-mm isotropic resolution were acquired at 3T and used as the anatomical substrate for the retinotopy data. See (Glasser et al. 2013) for full details.

Human functional scans. Whole-brain scans were collected using a T2*-sensitive gradient echo planar pulse sequence at a resolution of 1.6mm isotropic and 1s TR (multiband acceleration 5, in-plane acceleration 2, 85 slices). See (Glasser et al. 2013) for full details.

Macaque anatomical scans. A whole-brain structural volume was acquired while the animals were anesthetized with a combination of Ketamine (4mg/kg) and Dexdomitor (0.02mg/kg) and using a 15-channel transmit / receive knee coil. Monkeys were scanned using a T1w magnetization-prepared rapid gradient echo (MPRAGE) sequence; 0.5 x 0.5 x 0.5 resolution; FOV = 128 mm; 256 x 256 matrix; TR = 2700 ms; TE = 3.35 ms; TI = 859 ms; flip angle = 9°. 3 whole-brain anatomical images were collected in each animal.

Macaque functional scans. Whole-brain scans were collected using a T2*-sensitive gradient echo planar pulse sequence at a resolution of 1mm isotropic and 2s TR (in-plane acceleration 2, 67 slices). To enhance contrast (Vanduffel et al. 2001), we injected 12 mg/kg mono-crystalline iron oxide nanoparticles (Feraheme, AMAG Pharmaceuticals, Cambridge, MA) in the saphenous vein just before scanning. See Arcaro et al. 2017a for full details.

Data analyses. Data were analyzed using Human Connectome Workbench, Analysis of Functional NeuroImages (AFNI), SUMA, Freesurfer (Freesurfer), JIP Analysis Toolkit (written by Joseph Mandeville), and MATLAB (Mathworks).

Reconstruction of human cortical surfaces. White and pial cortical surfaces were reconstructed from the structural scans using the HCP Pipelines (Glasser et al., 2013). Surfaces were aligned across participants to the HCP 32k fs_LR standard surface space using a twofold approach. First, a gentle folding-based registration was used (referred to as “MSMSulc”). Second, a more aggressive areal feature-based registration was used (referred to as “MSMAll”). The latter approach is multi-modal in nature and uses myelin maps, resting-state network maps, and 3T resting-state visuotopic maps (Robinson et al. 2014, 2018; Glasser et al. 2016) to reconstruct cortical surfaces and align one to another.

Reconstruction of macaque cortical surfaces. Each animal’s 3 structural scans were co-registered and averaged. Each average structural volume underwent semi-automated cortical surface reconstruction using FreeSurfer. To ensure high accuracy, skull stripping and white matter masks were first manually segmented by an expert then passed into FreeSurfer’s autosegmentation pipeline. If poor segmentations were detected, the white matter mask and control points were edited, and surface reconstruction was rerun until corrected. To fix segmentation errors, average anatomical volumes were manually edited to improve the grey/white matter contrasts and to remove surrounding non-brain structures (e.g., sinuses, arachnoid and dura matter. See Arcaro et al. 2017a for more details).

Human functional data analyses. The data were processed using the HCP pipelines as previously published (Glasser et al. 2013), which correct for head motion and EPI distortion and register the functional data to individual participant surfaces. The time series data were analyzed using a population receptive field (pRF) model referenced as the Compressive Spatial Summation model (Kay et al. 2013; <http://cvnlab.net/analyzePRF>).

Macaque functional data analysis. The data were processed using AFNI. All images from each scan session were motion corrected and aligned to a single timepoint for that session. Data were detrended and spatially filtered using a Gaussian filter of 2 mm full-width at half-maximum (FWHM) to increase the signal-to-noise ratio (SNR) while preserving spatial specificity. Data were registered using a two-step linear then non-linear alignment approach (JIP analysis toolkit) to a standard anatomical template for all monkeys. Fourier analysis was used to identify spatially selective voxels from polar angle and eccentricity experiments. Results from this analysis approach were originally reported in Arcaro et al. 2017a and are further quantified in this paper.

Regions of interest (ROIs).

Identification of rCaS and eCaS. In humans, rCaS and eCaS were manually defined by a neuroanatomist (KSW) in each individual based on the most recent definitions (Iaria and Petrides 2007; Iaria et al. 2008; Petrides 2019). In monkeys, rCaS and eCaS were also identified by a neuroanatomist (KSW) guided by previous work (Van Essen et al. 1984; Horton and Hocking 1996; Galletti et al. 2001; Figure 7) and then manually defined by MJA.

Identification of V1. In both species, primary visual area V1 was identified as the region within the calcarine sulcus of occipital cortex that showed spatially specific retinotopic representations. Smooth, continuous representations of visual space were identified along the cortical surface for both polar angle and eccentricity mapping experiments in each individual human and macaque (Figure 2; Supplementary Figure 2). The border between V1 and V2 was identified by reversals in polar angle phase progression at the lower (Figure 2; blue colors in angle maps) and upper (red colors) visual fields in dorsal and ventral portions of the CaS, respectively. The lateral-medial extent of V1 was identified by a progression from the most foveal (Figure 2; red colors in eccentricity maps) to the most peripheral (blue colors) representations.

Cortical surface measurements.

Cortical surface area. For rCaS and eCaS, cortical surface area was measured along the pial surface segmentations using AFNI's SurfMeasures. Surface area was measured both in raw units (mm^2) and normalized to the total surface area of V1 in each participant (Supplementary Figure 3).

Distance from V1 foveal confluence. Cortical distance between each point (surface node) within V1 and the foveal confluence was estimated along pial surface segmentations using AFNI's SurfDist. Because the vertical meridian boundary between V1 and V2 is difficult to measure within the fovea using fMRI, the foveal confluence was defined as a curved line through the most foveal measurements linking the upper and lower vertical meridian boundaries identified within the surrounding parafoveal regions. Cortical distance from the fovea was defined as the

minimum Euclidean distance along the cortical surface between each V1 surface node and the foveal confluence line. Treating the foveal confluence as a single point defined at the midpoint along this line yielded qualitatively similar results for subsequent analyses and did not change interpretation of the data.

Cortical Magnification. For each participant, eccentricity measurements within V1 were plotted as a function of cortical distance from the foveal confluence. This produced a scatter plot where each data point represents a single surface node (Figure 6). An exponential curve as proposed in (Strasburger 2019; equation 16) was then fit to the data points:

$$E = a (e^{b\hat{d}} - 1)$$

where E is the predicted eccentricity (in deg), \hat{d} = cortical distance, and a and b are free parameters. The constant term (-1) allows for fitting foveal ($< 1^\circ$) measurements. The curve was fit using MATLAB's Curve Fit Tool, minimizing the sum of the squared errors between the actual eccentricity values and the eccentricity values predicted by the curve.

Visual field coverage.

The average eccentricity representation within both rCaS and eCaS was calculated for each participant. The group mean and standard error across participants were calculated. Polar angle and eccentricity measurements for each surface node were converted to Cartesian space (Matlab's pol2cart) and visualized in scatter plots for humans and macaques separately.

Statistical analyses.

We evaluated visual field coverage and areal size differences across species using two-way ANOVAs with species (humans/macaques) and hemisphere (right/left) as factors.

RESULTS

The retrocalcarine (rCaS) and external calcarine (eCaS) sulci were identified bilaterally in 24 humans and 6 macaques. In both species, the rCaS and eCaS were localized to the medial and lateral surfaces of occipital cortex, respectively. In both macaques and humans, the rCaS was located on the most posterior portion of the medial surface with the long axis oriented along the inferior-superior dimension. The macaque eCaS was located in the ventral half of the operculum of the occipital lobe with the long axis oriented along the posterior-anterior axis. The human eCaS was identified as the most posterior sulcus on the lateral surface of the occipital lobe as described in previous work (Iaria and Petrides 2007; Iaria et al. 2008; Petrides 2019). To examine the consistency and variability in the cortical position of these sulci across individuals, each individual's native surfaces were aligned to species-specific template surfaces (Figure 3). Group overlap maps were calculated across individuals and compared to the rCaS (black lines) and eCaS (white lines) identified on each group template. There was considerable overlap across individuals for both sulci with no confusability between sulci. For example, variability in the rCaS most often occurred anteriorly and superiorly, but remained on the medial surface, while variability in the eCaS most often occurred ventrally and anteriorly, but did not extend to the medial occipital surface. The group overlap maps were also projected into volumetric space for visual reference

(Figure 3). The presence of the rCaS and eCaS in each individual confirms that these sulci are prominent macroanatomical structures in both humans and macaques.

[Figure 3 Here]

In both humans and macaques, the rCaS and eCaS fell within V1 (Figure 4; Supplementary Figure 2). Consistent with prior imaging studies in humans (Engel et al. 1994, 1997; Sereno et al. 1995) and macaques (Brewer et al. 2002), V1 was identified in each hemisphere as a map of contralateral visual space within the CaS (Methods – Identification of visual area V1). In macaques, both the rCaS and eCaS fell entirely within V1 in each individual. In humans, the rCaS fell entirely within V1, but the eCaS fell at least partially outside of V1 for several participants (9 of 48 hemispheres). In both species, the surface area of the rCaS (average human: 163.11 mm² +/- 11.06; average macaque: 97.62 mm² +/- 5.83) was larger than the eCaS (average human: 41.49 mm² +/- 2.81; average macaque: 39.91 mm² +/- 3.08) and comprised a larger portion of V1's total surface area (Supplementary Figure 3; average human: 15.8% +/- 0.84 vs. 2.15% +/- 0.26; average macaque: 15.0% +/- 1.04 vs. 10.3% +/- 0.83). Notably, the size of the rCaS relative to V1 was similar between species (no significant main effects of species or hemispheres, $p > 0.05$), but the size of the eCaS relative to V1 was substantially larger in macaques than humans (significant main effect of species: $F(1,56)=151.59$, $p < 0.001$; no significant effect of hemisphere and no interaction, $p > 0.05$).

[Figure 4 Here]

The rCaS and eCaS were localized to specific parts of the retinotopic map in V1 (Figure 5). In both species, the eCaS preferred representations occupied by the central visual space, though the average visual field representations within the rCaS differed substantially between species (significant main effect of species: $F(1,56) = 541.07$, $p < 0.0001$; no significant effect of hemisphere and no interaction, $p > 0.05$). Across participants, the mean eccentricity representation of the eCaS was 0.40° (+/- 0.03) in humans and 2.45° (+/- 0.07) in macaques. In both species, the rCaS preferred representations occupied by more eccentric locations of visual space relative to the eCaS. However, the average visual field representations within the rCaS also differed substantially between species (significant main effect of species: $F(1,56) = 403.5$, $p < 0.0001$; no significant effect of hemisphere and no interaction, $p > 0.05$). Across participants, the mean eccentricity representation of the rCaS was 2.73° (+/- 0.13) in humans and 7.34° (+/- 0.06) in macaques. The differences in visual field coverage between humans and macaques were further apparent by visualizing the range of eccentricity representations within the eCaS, within the rCaS, and across the rest of V1 as a function of cortical distance from the foveal confluence (Figure 6). Differences in visual field coverage across species were apparent for both rCaS and eCaS. The eCaS covered a wider range of eccentricities in macaques than humans (significant main effect of species: $F(1,47)=725.37$, $p < 0.0001$; no effect of hemisphere or interaction, $p > 0.05$; Figure 6, Supplementary Figure 4; red dots and lines). The rCaS on the other hand covered a wider range of eccentricity representations in humans compared to macaques (significant main effect of species: $F(1,56)=10.82$, $p < 0.002$; no significant effect of hemisphere or interaction, $p > 0.05$; Figure 6, Supplementary Figure 4; blue dots and lines).

[Figure 5 Here]

Visual field coverage with respect to polar angle also differed between species for both sulci (Figure 3, right). In humans, the eCaS spanned upper and lower visual field representations with, if anything, a slight bias for lower visual field coverage. In macaques, the eCaS fell almost exclusively within upper visual field representations of V1. This visual field bias was also evident in the cortical surface images with the eCaS elongated parallel to the polar angle map (Figure 2). In humans, the rCaS covered more of the lower visual field representation (especially the most peripheral representations). In macaques, rCaS covered both the upper and lower visual field. Taken together, these macroanatomical landmarks are predictive of the functional organization of V1 *within species*, but not *across species*.

[Figure 6 Here]

The differences in visual field coverage of the rCaS and eCaS across species reflect a medial shift of V1's retinotopic map in humans relative to macaques. In humans, V1 was localized almost entirely to the medial surface with only the most foveal representations extending to the lateral surface. In monkeys, the central 6-7° was localized to the lateral opercular surface with peripheral representations localized to the medial surface. In addition to differences in V1's relative anatomical location across species, there were notable differences in the cortical morphology. Most of human V1 fell on concave cortical folds embedded within the large folds of the calcarine. In contrast, the opercular surface of V1 in macaques comprises a convex fold bulging out laterally (Figure 5; curvature views). Thus, the orientation of the V1 retinotopic map along the cortical surface is similar between humans and macaques. However, there are notable differences in the relation of cortical position and morphology of V1 across species.

DISCUSSION

“Above all, the striking fact that in Man almost the entire striate area is found buried in a long and deep calcarine fissure wholly, or almost wholly, located on the medial face of the hemisphere, whereas in the lower Primates not less than half of the striate area is spread over the lateral face of the occipital lobe, requires a satisfactory phylogenetical explanation.” (Polyak 1957), Pg. 467

Consistent with the classic quotation from Polyak (1957) above, modern measurements with functional magnetic resonance imaging (Brewer et al. 2002; Fize et al. 2003; Orban et al. 2004; Pinsk et al. 2005; Wandell et al. 2007; Goense et al. 2007; Wade et al. 2008; Wandell and Smirnakis 2009; Kolster et al. 2010, 2014; Arcaro et al. 2011, 2017b; Livingstone et al. 2017; Arcaro and Livingstone 2017) acknowledge that V1 is laterally displaced in macaques relative to humans. Nevertheless, to our knowledge, previous studies have not yet explicitly quantified this complex relationship between the anatomical and functional displacement of V1 between species using the same methodology. The retrocalcarine sulcus (rCaS) is an intriguing macroanatomical landmark to begin to fill in this gap in knowledge across species because morphologically, the rCaS is in the same macroanatomical location (on the medial surface of the cerebral cortex toward the occipital pole) and oriented similarly (vertically) in both macaques and humans. In the present study, we used anatomical and functional MRI to quantify the relationship between the rCaS and

the V1 eccentricity map between species. We chose to focus on eccentricity because previous neurophysiology studies show a predictable relationship between the rCaS and eccentricity representations in the macaque (Daniel and Whitteridge 1961; Van Essen et al. 1984; Horton and Hocking 1996; Galletti et al. 2001; Figure 7). Here, we also find a predictable relationship between the rCaS and eccentricity in humans, but the visual field coverage differed between species. We discuss these results in the context of i) how the same macroanatomical structure can be coupled with different functional representations between species and ii) phylogenetic and anatomical mechanisms that could account for this difference in sulcal-functional coupling between species.

[Figure 7 Here]

The same macroanatomical structure can be coupled with different functional representations between species

Morphologically, our results identify a vertical, or bifurcated, portion of the calcarine sulcus on the medial surface toward the occipital pole in human and non-human primates (Huxley 1861; Flower 1862; Cunningham 1892; Retzius 1896, 1906; Smith 1904a, b). Despite historical contentions regarding nomenclature in respect to this cortical expanse (Materials and Methods), we refer to this vertical portion of the calcarine sulcus as the retrocalcarine sulcus (rCaS), which is both consistent with classic (Smith 1904a, b) and modern (Iaria and Petrides 2007; Iaria et al. 2008; Petrides 2019) neuroanatomical studies, as well as is distinct from the laterally adjacent eCaS. Within species, our results show a correspondence between part of V1's retinotopic map and the rCaS (Figs. 2-4). Between species, our results show that this structure-function coupling is different between macaques and humans with the rCaS corresponding to more peripheral representations in macaques. Together, these results indicate that researchers can predict a range of eccentricity representations by locating the rCaS in individual hemispheres within each species: functionally, the rCaS represents eccentricities 2 (posterior lip of rCaS) to 5° (anterior lip of rCaS) in humans and 7 (posterior lip of rCaS) to 10° (anterior lip of rCaS) in macaques.

Our measurements are consistent with a handful of previous studies that have examined the relationship between the rCaS and eccentricity representations in non-human primates, reporting that the “hinge” of the operculum, which is just posterior to the rCaS, is ~7-8 degrees (Daniel and Whitteridge 1961; Van Essen et al. 1984; Horton and Hocking 1996; Galletti et al. 2001). We also emphasize that these prior studies used different labels to refer to the rCaS. For instance, Daniel and Whittredge (1961) referred to this portion of the calcarine based off of the fact that it resembled a “mushroom” that contains both a “head” and “stem” (the labels have been added to the image below). Van Essen and colleagues offered a slightly different strategy with independent labels for the “roof,” “dorsal leaf,” and “ventral leaf” of the rCaS. Horton and Hocking (1996) referred to the “hinge” of the operculum, which is located just posterior to the rCaS. Finally, Galletti et al. (2001) referred to the “posterior branch” of the calcarine, which is what we refer to as the rCaS.

To our knowledge, this is the first study to clearly show that the same macroanatomical structure (rCaS) can be coupled with different retinotopic representations between species (Figures 2-4). This is because the cortical positioning (on the medial surface of the cerebral cortex toward the occipital pole) and morphology (vertical bifurcation) of the rCaS is so similar in both macaques

and humans, but the relative position of V1's retinotopic map is shifted medially in humans. Nevertheless, we also acknowledge that the present findings may or may not extend to other anatomical locations in primary or association cortices, which can be tested in future research. For example, the parieto-occipital and calcarine sulci emerge at similar timepoints in gestation (Chi et al. 1977; Nishikuni and Ribas 2013). As a number of different retinotopic and functionally-specialized areas are located within the POS in both macaques and humans such as V6/PO (Colby et al. 1988; Galletti et al. 2001; Pitzalis et al. 2006, 2010, 2013; Glasser et al. 2016), area prostriata (Sanides and Vitzthum 1965; Sanides 1969; Glasser et al. 2016; Mikellidou et al. 2017), and a scene-selective region (Epstein 2008; Nasr et al. 2011; Epstein and Baker 2019), future studies can implement a similar approach as in the present study, but instead for cortical areas within the POS. Such an approach will determine if the present findings also extend to other primary sulci. Additionally, the intraparietal sulcus (IPS) is i) identifiable in both species, ii) contains a number of retinotopic and functionally-specialized areas between species, and iii) is morphologically dissociable between species. That is, the human IPS contains multiple components that are not present in the macaque IPS (Grefkes and Fink 2005; Zlatkina and Petrides 2014). Specifically, Grefkes and Fink (2005) write:

“The sulcal anatomy of a macaque brain is much less complicated than the highly gyrified cortex of a human brain. The IPS in humans often has various side branches...and shows a complex folding pattern...through posterior portions of the IPS” (Pg. 4).

These various side branches have since been named (Zlatkina and Petrides 2014; Petrides 2019). Thus, future studies can compare sulcal-functional correspondence between species in the IPS, while also taking into consideration the morphological differences of the IPS between species. And while we use the POS and IPS as examples of sulci in primary and association cortices, respectively, this approach can be applied to any sulcus present in both species in any cortical expanse.

Potential phylogenetic and anatomical mechanisms explaining how the same macroanatomical structure can be coupled with different functional representations between species

Our findings support an interpretation that nearly all of the V1 map is shifted medially in human occipital cortex relative to macaques (Fig. 7E) and cannot be explained by substantial differences in cortical magnification such as an expanded foveal representation in humans (Fig. 6). This is particularly notable given the relatively rigid constraints guiding thalamocortical projections to primary sensory areas early in development. What might explain this difference in anatomical-functional mapping between species? First, we consider a phylogenetic explanation and then a mechanistic anatomical explanation. Consistent with the Introductory quotation to this Discussion, Polyak (1957) proposed a 6-phase phylogenetic explanation as to why V1 is buried within the human CaS on the medial surface of the occipital cortex and why a bulk of V1 is displaced and spread over the lateral face of the occipital lobe in macaque. Despite this difference, there is what he referred to as a “complete retinotopical homology” (Polyak, 1957, pg. 467) between the posterior 1/3 of the human calcarine and the macaque operculum. Briefly, Polyak (1957) proposed that the change from an arboreal (macaque) to a terrestrial (human) way of life put a demand on vision. In response to this demand, there was a decline and recession of the operculum with increased gyrification and folding. Polyak (1957) writes:

“...the original simian occipital lobe or occipital operculum was rolled back, and the lateral portion of the striate area displaced backward and rolled in to form the lateral or posterior calcarine sulcus of the hominoid and hominid brain (lc)” (pg. 470).

It is likely that underlying changes in microarchitecture and connectivity correspond with Polyak’s proposed phylogenetic changes. For example, the location of V1 was recently discussed relative to differences in myelination and connectivity associated with the expansion of temporal association cortices from macaques to chimpanzees to humans (Bryant et al. 2019). Specifically, Bryant and colleagues write:

“Note that the relative proportions of lightly myelinated cortex in temporal cortex...increase dramatically from macaques to chimpanzees to humans. In humans, this increase is accompanied by a posterior and inferior displacement of the extrastriate cortex, so that the MT complex (areas MT, MST, and FST) is located posterior to the STS, and very little of area V1 extends onto the lateral surface of the occipital lobe.”

Co-occurring with this displacement is an increase in myelination on the medial surface of the occipital lobe in humans compared to macaques and chimpanzees. Additionally, the foveal portion of V1 shows different long-range connectivity in humans and chimpanzees compared to macaques (Bryant et al., 2019). Specifically, humans and chimpanzees, but not macaques, show long-range anatomical connectivity among the foveal portions of V1 and anterior, inferior, and lateral portions of temporal cortices when using diffusion MRI and tractography analyses (Bryant et al., 2019). These findings are consistent with tract-tracing studies in macaques showing weak connections between V1 and areas in anterior, inferior, and lateral portions of temporal cortices (Doty 1983; Felleman and Van Essen 1991; Rockland and Van Hoesen 1994; Rockland et al. 1994; Gattass et al. 2005; Markov et al. 2011, 2014). Nevertheless, the fact that chimpanzees still exhibit i) a prominent lunate sulcus and ii) a laterally displaced V1 suggests that the “rolling back and folding in” (to paraphrase Polyak) of striate cortex was a gradual evolutionary change, which can be further explored in future studies.

Causal support for this relationship among connectivity, cortical folding, and the microarchitecture of V1 extends from classic (Rakic 1988; Dehay et al. 1989, 1996; Rakic et al. 1991) and modern (Magrou et al. 2018) studies examining the effects of enucleation during different stages of development and the connectivity and microarchitecture of V1, as well as the morphology of the calcarine sulcus and the operculum. Specifically, enucleation influences the folding of the operculum, as well as the cytoarchitecture and morphology of the portion of V1 within the rCaS (Dehay et al. 1989, 1996). In terms of cortical folding, 5-8 “new” sulci can appear on the operculum that are not present in typically developing macaques (Dehay et al. 1996). Relatedly, enucleation influences thalamocortical and cortico-cortical connections of the developing macaque brain (Magrou et al. 2018). As morphological and connectivity features (Butt et al. 2013; Bock et al. 2015; Andelin et al. 2019) of V1 are also different between blind and sighted human participants, future studies comparing the morphology of the rCaS between blind and sighted participants, as well as using the rCaS as a seed in anatomical and functional connectivity analyses, would serve as a natural next step building on the present and previous work in both humans and non-human primates.

We further highlight that microarchitecture and connectivity also likely contribute to the consistency in the sulcal-functional mapping identified here. For example, previous measurements show a consistent topological relationship between polar angle representations and transcallosal connections in both monkeys and humans. In monkeys, a number of studies showed that transcallosal fibers terminate along the vertical meridia separating a series of visual areas, the most relevant of which for the present paper is the V1/V2 boundary (Zeki 1977; Van Essen et al. 1982; Burkhalter et al. 1986; Kennedy et al. 1986; Felleman et al. 1997). In humans, studies implementing either dMRI and tractography (Dougherty et al. 2005) or polarized light imaging (Caspers et al. 2015) identified structure-function relationships between topological positions within the splenium of the corpus callosum and topological positions of the CaS. Additionally, the V1/V2 border has distinctive myeloarchitectonic (Sanides and Vitzthum 1965; Caspers et al. 2015) and cytoarchitectonic (von Economo and Koskinas 1925; Amunts et al. 2000) features. Thus, the relationship among polar angle representations, connectivity, and microarchitecture can now be revisited when also considering the rCaS in future studies in either species.

CONCLUSION

Here, we examined the structural-functional relationship between the retrocalcarine sulcus (rCaS) and the functional maps within V1 in macaques and humans using anatomical and functional MRI. We find a consistent sulcal-functional relationship across individuals separately within each species, but a different sulcal-functional relationship among individuals between species. Specifically, the rCaS represents eccentricities 2-5° in humans, but 7-10° in macaques. These results indicate that the same macroanatomical structure can be coupled with different functional representations between species. Likely inter-related phylogenetic and anatomical mechanisms contribute to the fact that the same macroanatomical structure can be coupled with different functional representations between species. Future studies examining whether sulcal-functional mappings also diverge in other cortical regions will help us better understand the development and evolution of the cerebral cortex across species.

CAPTIONS TO FIGURES

Figure 1. The retrocalcarine sulcus (rCaS) in the primate occipital cortex and *in utero*. (A) In the first labeling of the calcarine sulcus (*l* in each image) in 1861, Sir Thomas Huxley referred to the fact that there was a bifurcation (dotted red line) in the posterior extent toward the occipital pole in both spider monkeys (*Ateles*; left) and humans (middle). Right: Coronal sections from *Ateles* (top; A') and humans (bottom; A) in which the bifurcated portion of the posterior calcarine sulcus was described by Huxley. Images adapted from Huxley, 1861. (B) Shortly after Huxley's seminal observations, several labels were proposed for this posterior bifurcation of the CaS. For example, in a series of papers, Smith (1904a) referred to this sulcus with several names such as sulcus retrocalcarinus verticalis (Smith 1902), the retrocalcarine sulcus (Smith, 1904a), the sulcus occipitalis intrastriatus mesialis (retrocalcarinus) (Smith 1904b), or simply as r3 as depicted in the two leftmost images. Images adapted from Smith, 1904a. (C) The rCaS (dotted red line) is identifiable in several species included in the classic atlas by Retzius (1906). Left to right: baboon, capuchin, and chimpanzee. Images adapted from Retzius (1906). (D) Left and middle: Drawings of two separate brains from early (left) or the middle (middle) of the 5th month of development. Cunningham referred to the rCaS as the posterior calcarine (*c*³ in the images). Images Adapted from Cunningham (1892). Right: A photograph of a fetal brain from Retzius (1896). The rCaS (dotted red) is easily identifiable, as is the external calcarine (unlabeled), which is posterior to the rCaS. Images adapted from Retzius (1896).

Figure 2. The rCaS is difficult to identify in flattened and inflated cortical surface visualizations. Medial views of the pial surface from the right and left hemispheres of an example participant (randomly chosen) from our 181 human participants. The portions of cortex in the dotted square have been computationally flattened. The labeling of sulci a-c is aimed to guide the reader in identifying corresponding sulci across views. While the rCaS (dotted red) is clearly visible on the pial surface, the flattening process often distorts the clear bifurcated morphology of the rCaS, which makes it hard to discriminate from the rest of the calcarine or the external calcarine sulci (green dotted line in the right hemisphere).

Figure 3. Anatomical localization of the rCaS and eCaS in human and macaque. (Left) Sagittal and coronal slices of group overlap maps for rCaS (red) and eCaS (blue) for (Top) humans and (Bottom) macaques. Group overlap maps range from most (bright colors) to least (dark colors) overlap. (Right) Group overlap maps for rCaS and eCaS shown on inflated and pial cortical surface views of macaque (NMT) and human (fsaverage) template surfaces. Colormap ranges from 1/n to n.

Figure 4. Retinotopic organization of the retrocalcarine sulcus (rCaS) and external calcarine sulcus (eCaS) relative to V1 in humans and macaques. Outlines of the group-defined rCaS (black solid line) and eCaS (white solid line) and individual-defined rCaS (dark pink solid line) and eCaS (light pink solid line) on cortical surface curvature, polar angle, and eccentricity maps in humans (top) and macaques (bottom). Group averaged (left) and individual participant (right) data are shown. White dotted lines illustrate the borders between visual areas V1 and V2. To help relate the lateral and medial viewpoints of the macaque surfaces, green and yellow asterisks mark corresponding locations in V1. See Supplementary Figure 2 for more example participants.

Figure 5. Visual field coverage of rCaS and eCaS in humans and macaques. (Left) The mean eccentricity representation within the rCaS (blue) and eCaS (red) for individuals (grey circles) and group averages (black circles) in humans (Top) and macaques (Bottom). (Right) Visual field coverage in Cartesian space of each surface node within the rCaS and eCaS across all participants.

Figure 6. Eccentricity representations of rCaS and eCaS as a function of cortical distance in humans and macaques. (Left) Exponential curve fits to eccentricity as a function of cortical distance from V1's foveal confluence for each individual (Top) human and (Bottom) macaque. The range of eccentricity and cortical distances covered by the rCaS (blue line) and eCaS (red line) are shown relative to the rest of V1 (grey line). (Right) Scatter plots of eccentricity representations in relation to cortical distance from V1's fovea within the rCaS (blue), the eCaS (red), and the rest of V1 (grey) for three individuals. The range of eccentricity and cortical distances covered by the rCaS and eCaS are illustrated by red and blue dashed lines, respectively. See Supplementary Figure 4 for additional example individuals.

Figure 7. Eccentricity and the rCaS across species, methods, and time (1961-2021). (A) A drawing from Daniel and Whittredge (1961) of a baboon's brain. Needle tracks (vertical black lines) are depicted relative to cortical locations that reflect the preferred neuronal firing to spots of light at a particular radial distance from the fixation point (numbers). (B) *Left:* A drawing of a coronal slice from a macaque brain showing different parts of the rCaS (roof, ventral leaf, and dorsal leaf; Van Essen et al., 1984). *Right, Bottom:* Drawings of flattened versions of V1 with labeled eccentricity values relative to the three pieces of the rCaS. Images adapted from Van Essen et al., 1984. (C) *Left:* A flattened version of V1 stained with cytochrome oxidase and labeled with eccentricity values, in which the arrow denotes 8° . *Right:* A schematic version of the leftmost image. Images adapted from Horton and Hocking, 1996. (D) A drawing of a macaque brain, slightly rotated and labeled with eccentricity values in which 7° is just posterior to the rCaS (labeled here as "posterior branch") from Galletti et al., 2001. (E) Eccentricity maps on inflated cortical surfaces for (left) macaques and (right) humans from the present group average data.

REFERENCES

- Amunts K, Malikovic A, Mohlberg H, et al (2000) Brodmann's areas 17 and 18 brought into stereotaxic space-where and how variable? *Neuroimage* 11:66–84.
- Andelin AK, Olavarria JF, Fine I, et al (2019) The Effect of Onset Age of Visual Deprivation on Visual Cortex Surface Area Across-Species. *Cereb Cortex* 29:4321–4333.
- Arcaro MJ, Kastner S (2015) Topographic organization of areas V3 and V4 and its relation to supra-areal organization of the primate visual system. *Vis. Neurosci.* 32(e015): 1-15.
- Arcaro MJ, Livingstone MS (2017) A hierarchical, retinotopic proto-organization of the primate visual system at birth. *Elife* 6 (e26196):1-24.
- Arcaro MJ, Pinsk MA, Li X, Kastner S (2011) Visuotopic organization of macaque posterior parietal cortex: A functional magnetic resonance imaging study. *J Neurosci* 31:2064–2078.
- Arcaro MJ, Schade PF, Vincent JL, et al (2017) Seeing faces is necessary for face-domain formation. *Nat Neurosci* 20:1404–1412.
- Armstrong E, Schleicher A, Omran H, et al (1995) The ontogeny of human gyrification. *Cereb Cortex* 5:56–63
- Benson NC, Jamison KW, Arcaro MJ, et al (2018) The Human Connectome Project 7 Tesla retinotopy dataset: Description and population receptive field analysis. *J Vis* 18:1–22.
- Bock AS, Binda P, Benson NC, et al (2015) Resting-state retinotopic organization in the absence of retinal input and visual experience. *J Neurosci* 35:12366–12382.
- Brewer AA, Press WA, Logothetis NK, Wandell BA (2002) Visual areas in macaque cortex measured using functional magnetic resonance imaging. *J Neurosci* 22:10416–10426.
- Bryant KL, Glasser MF, Li L, et al (2019) Organization of extrastriate and temporal cortex in chimpanzees compared to humans and macaques. *Cortex* 118:223–243.
- Burkhalter A, Felleman DJ, Newsome WT, Van Essen DC (1986) Anatomical and physiological asymmetries related to visual areas V3 and VP in macaque extrastriate cortex. *Vision Res* 26:63–80.
- Butt OH, Benson NC, Datta R, Aguirre GK (2013) The fine-scale functional correlation of striate cortex in sighted and blind people. *J Neurosci* 33:16209–16219.
- Caspers S, Axer M, Caspers J, et al (2015) Target sites for transcallosal fibers in human visual cortex - A combined diffusion and polarized light imaging study. *Cortex* 72:40–53.
- Chi JG, Dooling EC, Gilles FH (1977) Gyral development of the human brain. *Ann Neurol* 1:86–93.
- Colby CL, Gattass R, Olson CR, Gross CG (1988) Topographical organization of cortical afferents to extrastriate visual area PO in the macaque: A dual tracer study. *J Comp Neurol* 269:392–413.
- Cunningham DJ (1892) *Contribution to the Surface Anatomy of the Cerebral Hemispheres.* Academy House, Dublin.
- Daniel PM, Whitteridge D (1961) *THE REPRESENTATION OF THE VISUAL FIELD ON*

THE CEREBRAL CORTEX IN MONKEYS. *J Physiol* 159(2): 203-221.

- Dehay C, Giroud P, Berland M, et al (1996) Contribution of thalamic input to the specification of cytoarchitectonic cortical fields in the primate: Effects of bilateral enucleation in the fetal monkey on the boundaries, dimensions, and gyrification of striate and extrastriate cortex. *J Comp Neurol* 367:70–89.
- Dehay C, Horsburgh G, Berland M, et al (1989) Maturation and connectivity of the visual cortex in monkey is altered by prenatal removal of retinal input. *Nature* 337:265–267.
- Doty RW (1983) Nongeniculate afferents to striate cortex in macaques. *J Comp Neurol* 218:159–173.
- Dougherty RF, Ben-Shachar M, Bammer R, et al (2005) Functional organization of human occipital-callosal fiber tracts. *Proc Natl Acad Sci U S A* 102:7350–7355.
- Elliot Smith C (1902) On the Morphology of the Brain in the Mammalia. *Transactions of the Linnean Society of London* 8: 386.
- Engel SA, Glover GH, Wandell BA (1997) Retinotopic organization in human visual cortex and the spatial precision of functional MRI. *Cereb Cortex* 7:181–192
- Engel SA, Rumelhart DE, Wandell BA, et al (1994) fMRI of human visual cortex. *Nature* 369:525
- Epstein RA (2008) Parahippocampal and retrosplenial contributions to human spatial navigation. *Trends Cogn Sci* 12(10): 388-396.
- Epstein RA, Baker CI (2019) Scene Perception in the Human Brain. *Annu. Rev. Vis. Sci.* 5:373–397
- Felleman DJ, Burkhalter A, Van Essen DC (1997) Cortical connections of areas V3 and VP of macaque monkey extrastriate visual cortex. *J Comp Neurol* 379:21–47.
- Felleman DJ, Van Essen DC (1991) Distributed hierarchical processing in the primate cerebral cortex. *Cereb Cortex* 1:1–47
- Fize D, Vanduffel W, Nelissen K, et al (2003) The retinotopic organization of primate dorsal V4 and surrounding areas: A functional magnetic resonance imaging study in awake monkeys.
- Flower WH (1862) IX. On the posterior lobes of the cerebrum of the quadrumana. *Philos Trans R Soc London* 152:185–201.
- Galletti C, Gamberini M, Kutz DF, et al (2001) The cortical connections of area V6: An occipito-parietal network processing visual information. *Eur J Neurosci* 13:1572–1588.
- Gattass R, Nascimento-Silva S, Soares JGM, et al (2005) Cortical visual areas in monkeys: Location, topography, connections, columns, plasticity and cortical dynamics. *Philos Trans R Soc B Biol Sci* 360:709–731.
- Glasser MF, Coalson TS, Robinson EC, et al (2016) A multi-modal parcellation of human cerebral cortex. *Nature* 536:171–178.
- Glasser MF, Sotiropoulos SN, Wilson JA, et al (2013) The minimal preprocessing pipelines for the Human Connectome Project. *Neuroimage* 80:105–124.
- Goense JBM, Zappe AC, Logothetis NK (2007) High-resolution fMRI of macaque V1. *Magn Reson Imaging* 25:740–747.

- Grefkes C, Fink GR (2005) The functional organization of the intraparietal sulcus in humans and monkeys. *J. Anat.* 207:3–17
- Horton JC, Hocking DR (1996) Intrinsic variability of ocular dominance column periodicity in normal macaque monkeys. *J Neurosci* 16:7228–7339.
- Huxley TH (1861) On the brain of *Ateles paniscus*. *Proc Zool Soc Lond* 249–260
- Iaria G, Petrides M (2007) Occipital sulci of the human brain: variability and probability maps. *J Comp Neurol* 501:243–259.
- Iaria G, Robbins S, Petrides M (2008) Three-dimensional probabilistic maps of the occipital sulci of the human brain in standardized stereotaxic space. *Neuroscience* 151:174–185.
- Kay KN, Winawer J, Mezer A, Wandell BA (2013) Compressive spatial summation in human visual cortex. *J Neurophysiol* 110:481–494.
- Kennedy H, Dehay C, Bullier J (1986) Organization of the callosal connections of visual areas v1 and v2 in the macaque monkey. *J Comp Neurol* 247:398–415.
- Kolster H, Janssens T, Orban GA, Vanduffel W (2014) The retinotopic organization of macaque occipitotemporal cortex anterior to V4 and caudoventral to the middle temporal (MT) cluster. *J Neurosci* 34:10168–10191.
- Kolster H, Peeters R, Orban GA (2010) The retinotopic organization of the human middle temporal area MT/V5 and its cortical neighbors. *J Neurosci* 30:9801–9820
- Livingstone MS, Vincent JL, Arcaro MJ, et al (2017) Development of the macaque face-patch system. *Nat Commun* 8: 1-12.
- Magrou L, Barone P, Markov NT, et al (2018) How areal specification shapes the local and interareal circuits in a macaque model of congenital blindness. *Cereb Cortex* 28:3017–3034.
- Markov NT, Ercsey-Ravasz MM, Ribeiro Gomes AR, et al (2014) A weighted and directed interareal connectivity matrix for macaque cerebral cortex. *Cereb Cortex* 24:17–36.
- Markov NT, Misery P, Falchier A, et al (2011) Weight consistency specifies regularities of macaque cortical networks. *Cereb Cortex* 21:1254–1272.
- Mikellidou K, Kurzawski JW, Frijia F, et al (2017) Area Prostriata in the Human Brain. *Curr Biol* 27:3056-3060.e3.
- Nasr S, Liu N, Devaney KJ, et al (2011) Scene-selective cortical regions in human and nonhuman primates. *J Neurosci* 31:13771–13785.
- Nishikuni K, Ribas GC (2013) Study of fetal and postnatal morphological development of the brain sulci: Laboratory investigation. *J Neurosurg Pediatr* 11:1–11.
- Orban GA, Van Essen D, Vanduffel W (2004) Comparative mapping of higher visual areas in monkeys and humans. *Trends Cogn. Sci.* 8:315–324
- Petrides M (2019) Atlas of the morphology of the human cerebral cortex on the average MNI brain. Academic Press, London.
- Pinsk MA, Moore T, Richter MC, et al (2005) Methods for functional magnetic resonance imaging in normal and lesioned behaving monkeys. *J Neurosci Methods* 143:179–195.
- Pitzalis S, Galletti C, Huang RS, et al (2006) Wide-field retinotopy defines human cortical visual area V6. *J Neurosci* 26:7962–7973.

- Pitzalis S, Sereno MI, Committeri G, et al (2013) The human homologue of macaque area V6A. *Neuroimage* 82:517–530.
- Pitzalis S, Sereno MI, Committeri G, et al (2010) Human v6: the medial motion area. *Cereb Cortex* 20:411–424
- Polyak S (1957) *The vertebrate visual system*. University of Chicago Press, Chicago, IL
- Rakic P (1988) Specification of cerebral cortical areas. *Science* (80-) 241:170–176.
- Rakic P, Suñer I, Williams RW (1991) A novel cytoarchitectonic area induced experimentally within the primate visual cortex. *Proc Natl Acad Sci U S A* 88:2083–2087.
- Retzius G (1906) *Cerebra simiarum illustrata. Das affenhirn in bildlicher darstellung*. G. Fischer, Stockholm
- Retzius G (1896) *Das Menschenhirn. Studien in der makroskopischen Morphologie*. Kgl. Buchdr. P. A. Norstedt and Söner, Stockholm
- Robinson EC, Garcia K, Glasser MF, et al (2018) Multimodal surface matching with higher-order smoothness constraints. *Neuroimage* 167:453–465.
- Robinson EC, Jbabdi S, Glasser MF, et al (2014) MSM: A new flexible framework for multimodal surface matching. *Neuroimage* 100:414–426.
- Rockland KS, Saleem KS, Tanaka K (1994) Divergent feedback connections from areas V4 and TEO in the macaque. *Vis Neurosci* 11:579–600.
- Rockland KS, Van Hoesen GW (1994) Direct temporal-occipital feedback connections to striate cortex (V1) in the macaque monkey. *Cereb Cortex* 4:300–313.
- Rosa MGP, Tweedale R (2005) Brain maps, great and small: Lessons from comparative studies of primate visual cortical organization. *Philos. Trans. R. Soc. B Biol. Sci.* 360:665–691
- Sanides F (1969) COMPARATIVE ARCHITECTONICS OF THE NEOCORTEX OF MAMMALS AND THEIR EVOLUTIONARY INTERPRETATION. *Ann N Y Acad Sci* 167:404–423.
- Sanides F, Vitzthum HG (1965) Zur Architektonik der menschlichen Sehrinde und den Prinzipien ihrer Entwicklung. *Dtsch Z Nervenheilkd* 187:680–707.
- Sereno MI, Dale AM, Reppas JB, et al (1995) Borders of multiple visual areas in humans revealed by functional magnetic resonance imaging. *Science* (80-) 268:889–893
- Sietz J (1886) Zwei Feuerlander-Gehirne. *Z Ethnol* 18: 237-284.
- Smith GE (1903) X. On the Morphology of the Brain in the Mammalia, with Special Reference to that of the Lemurs, Recent and Extinct. *Trans Linn Soc London 2nd Ser Zool* 8:319–432.
- Smith GE (1904a) Studies of the morphology of the human brain with special reference to that of Egyptians. No. 1. The occipital region. *Rec Egypt Govt Sch Med* 2:125–173
- Smith GE (1904b) The Morphology of the Occipital Region of the Cerebral Hemisphere in Man and the Apes. *Anatomscher Anzeiger* 24:436–451
- Strasburger H (2019) On the cortical mapping function – visual space, cortical space, and crowding. *bioRxiv* 621458
- Van Essen DC, Donahue CJ, Glasser MF (2018) Development and Evolution of Cerebral and

Cerebellar Cortex. *Brain Behav Evol* 91:158–169.

- Van Essen DC (2007) Cerebral Cortical Folding Patterns in Primates: Why They Vary and What They Signify. *Evol Nerv Syst* 267–276
- Van Essen DC, Glasser MF (2018) Parcellating Cerebral Cortex: How Invasive Animal Studies Inform Noninvasive Mapmaking in Humans. *Neuron* 99:640–663
- Van Essen DC, Newsome WT, Bixby JL (1982) The pattern of interhemispheric connections and its relationship to extrastriate visual areas in the macaque monkey. *J Neurosci* 2:265–283.
- Van Essen DC, Newsome WT, Maunsell JHR (1984) The visual field representation in striate cortex of the macaque monkey: Asymmetries, anisotropies, and individual variability. *Vision Res* 24:429–448.
- Vanduffel W, Fize D, Mandeville JB, et al (2001) Visual motion processing investigated using contrast agent-enhanced fMRI in awake behaving monkeys. *Neuron* 32:565–577.
- von Economo C, Koskinas GN (1925) *Die Cytoarchitektonik der Hirnrinde des erwachsenen Menschen*. Springer, Wien, Berlin
- Wade A, Augath M, Logothetis N, Wandell B (2008) fMRI measurements of color in macaque and human. *J Vis* 8(10):1-19.
- Wandell BA, Dumoulin SO, Brewer AA (2007) Visual field maps in human cortex. *Neuron* 56:366–383
- Wandell BA, Smirnakis SM (2009) Plasticity and stability of visual field maps in adult primary visual cortex. *Nat. Rev. Neurosci.* 10:873–884
- Zeki SM (1977) Simultaneous anatomical demonstration of the representation of the vertical and horizontal meridians in areas V2 and V3 of rhesus monkey visual cortex. *Proc R Soc London - Biol Sci* 195:517–523.
- Zilles K, Palomero-Gallagher N, Amunts K (2013) Development of cortical folding during evolution and ontogeny. *Trends Neurosci* 36:275–284.
- Zlatkina V, Petrides M (2014) Morphological patterns of the intraparietal sulcus and the anterior intermediate parietal sulcus of Jensen in the human brain. *Proc R Soc B Biol Sci* 281:1–8.

Figures

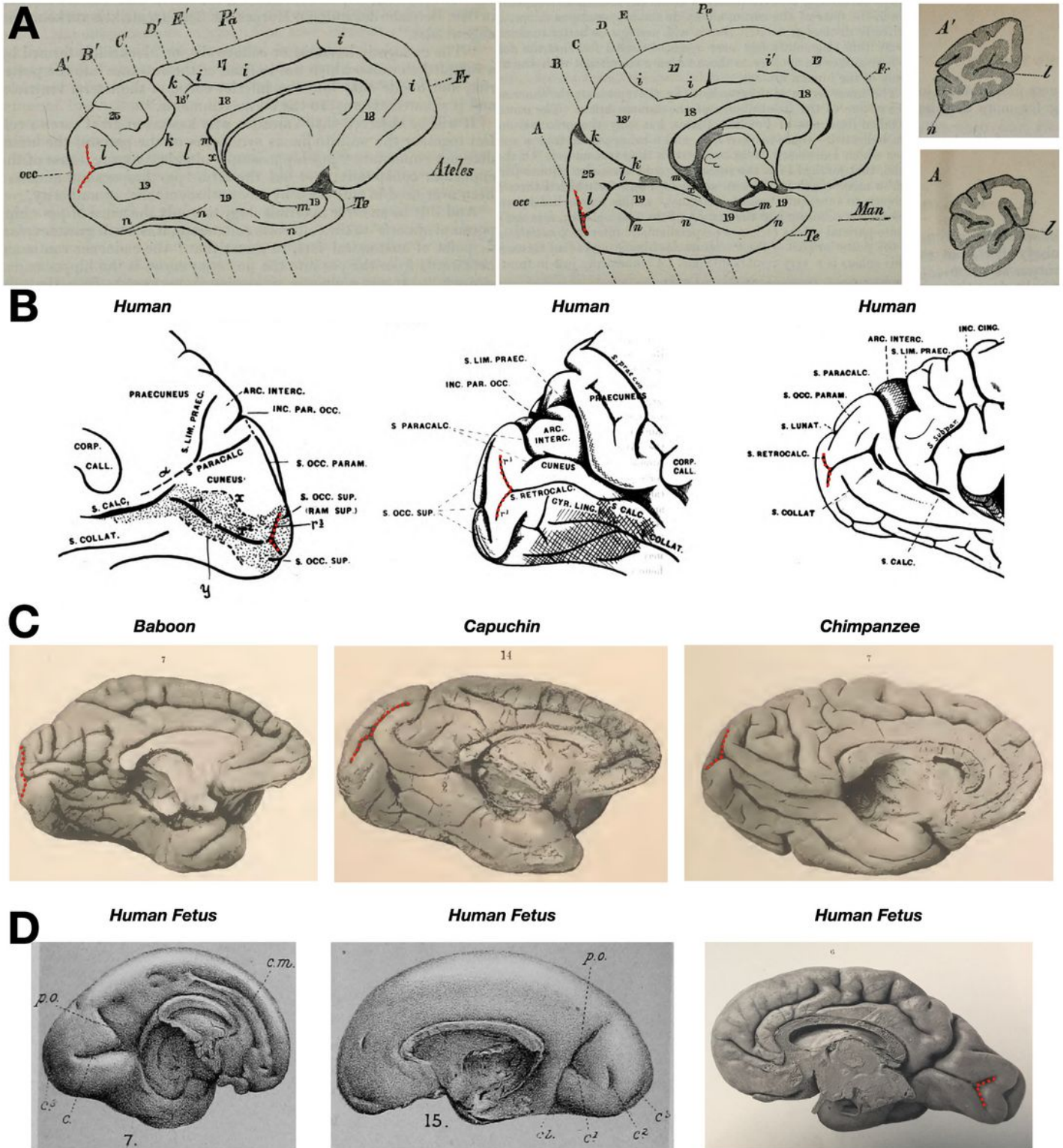


Figure 1

The retrocalcarine sulcus (rCaS) in the primate occipital cortex and in utero. (A) In the first labeling of the calcarine sulcus (l in each image) in 1861, Sir Thomas Huxley referred to the fact that there was a bifurcation (dotted red line) in the posterior extent toward the occipital pole in both spider monkeys

(Ateles; left) and humans (middle). Right: Coronal sections from Ateles (top; A') and humans (bottom; A) in which the bifurcated portion of the posterior calcarine sulcus was described by Huxley. Images adapted from Huxley, 1861. (B) Shortly after Huxley's seminal observations, several labels were proposed for this posterior bifurcation of the CaS. For example, in a series of papers, Smith (1904a) referred to this sulcus with several names such as sulcus retrocalcarinus verticalis (Smith 1902), the retrocalcarine sulcus (Smith, 1904a), the sulcus occipitalis intrastriatus mesialis (retrocalcarinus) (Smith 1904b), or simply as r3 as depicted in the two leftmost images. Images adapted from Smith, 1904a. (C) The rCaS (dotted red line) is identifiable in several species included in the classic atlas by Retzius (1906). Left to right: baboon, capuchin, and chimpanzee. Images adapted from Retzius (1906). (D) Left and middle: Drawings of two separate brains from early (left) or the middle (middle) of the 5th month of development. Cunningham referred to the rCaS as the posterior calcarine (c3 in the images). Images Adapted from Cunningham (1892). Right: A photograph of a fetal brain from Retzius (1896). The rCaS (dotted red) is easily identifiable, as is the external calcarine (unlabeled), which is posterior to the rCaS. Images adapted from Retzius (1896).

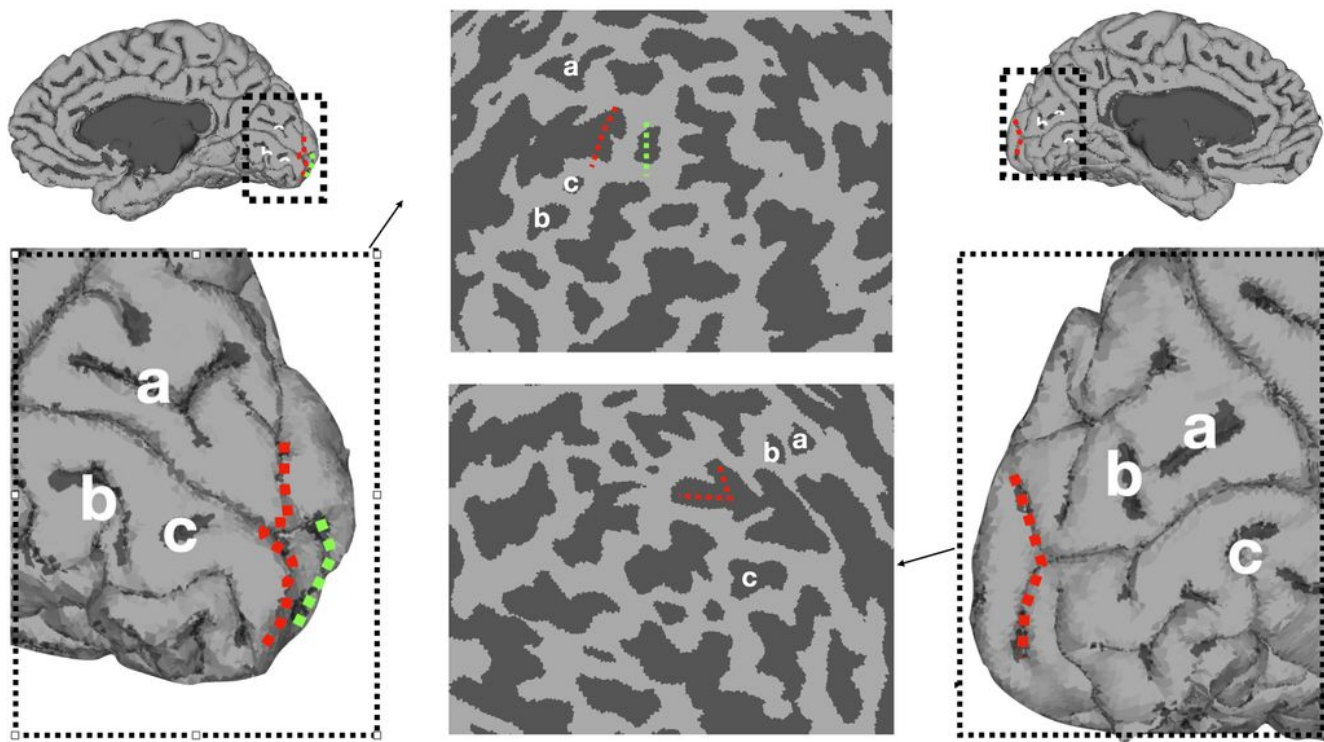


Figure 2

The rCaS is difficult to identify in flattened and inflated cortical surface visualizations. Medial views of the pial surface from the right and left hemispheres of an example participant (randomly chosen) from our 181 human participants. The portions of cortex in the dotted square have been computationally flattened. The labeling of sulci a-c is aimed to guide the reader in identifying corresponding sulci across views. While the rCaS (dotted red) is clearly visible on the pial surface, the flattening process often

distorts the clear bifurcated morphology of the rCaS, which makes it hard to discriminate from the rest of the calcarine or the external calcarine sulci (green dotted line in the right hemisphere).

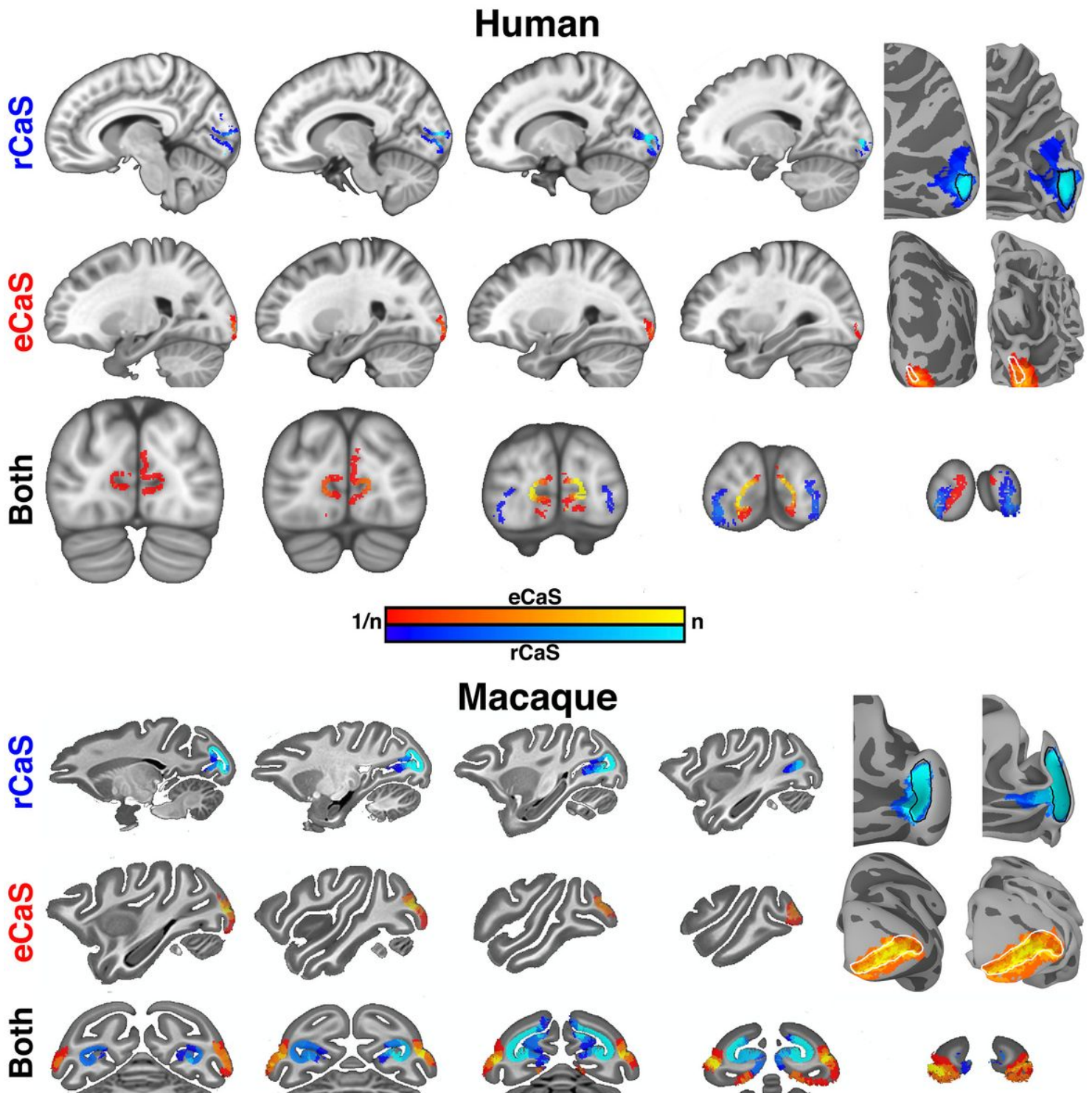


Figure 3

Anatomical localization of the rCaS and eCaS in human and macaque. (Left) Sagittal and coronal slices of group overlap maps for rCaS (red) and eCaS (blue) for (Top) humans and (Bottom) macaques. Group overlap maps range from most (bright colors) to least (dark colors) overlap. (Right) Group overlap maps

for rCaS and eCaS shown on inflated and pial cortical surface views of macaque (NMT) and human (fsaverage) template surfaces. Colormap ranges from $1/n$ to n .

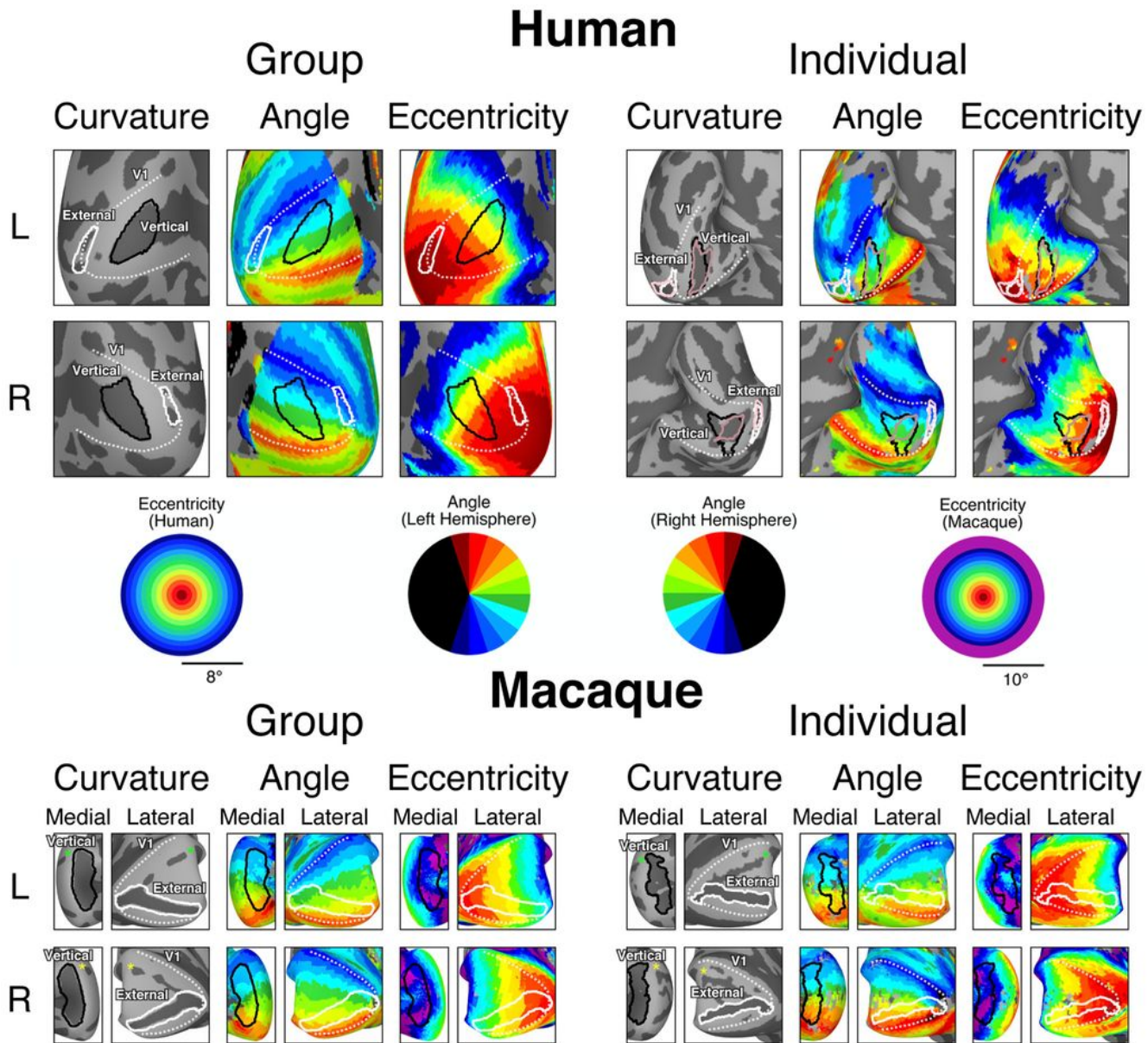
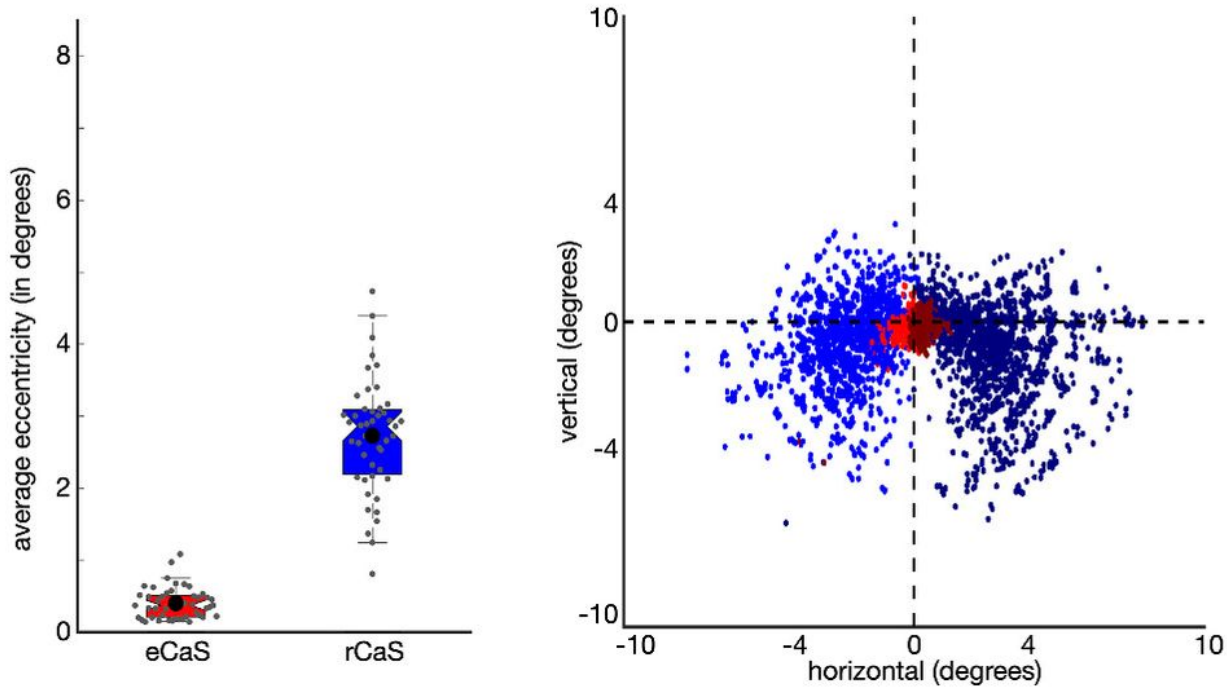


Figure 4

Retinotopic organization of the retrocalcarine sulcus (rCaS) and external calcarine sulcus (eCaS) relative to V1 in humans and macaques. Outlines of the group-defined rCaS (black solid line) and eCaS (white solid line) and individual-defined rCaS (dark pink solid line) and eCaS (light pink solid line) on cortical

surface curvature, polar angle, and eccentricity maps in humans (top) and macaques (bottom). Group averaged (left) and individual participant (right) data are shown. White dotted lines illustrate the borders between visual areas V1 and V2. To help relate the lateral and medial viewpoints of the macaque surfaces, green and yellow asterisks mark corresponding locations in V1. See Supplementary Figure 2 for more example participants.

Human



Macaque

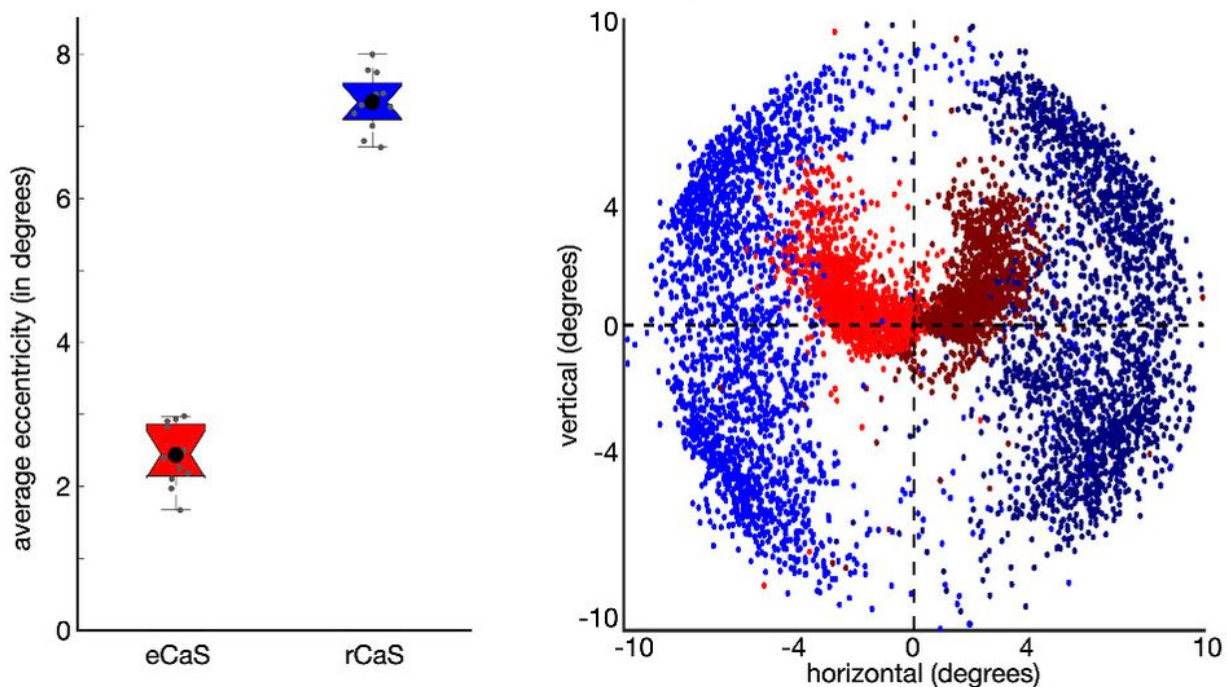


Figure 5

Visual field coverage of rCaS and eCaS in humans and macaques. (Left) The mean eccentricity representation within the rCaS (blue) and eCaS (red) for individuals (grey circles) and group averages (black circles) in humans (Top) and macaques (Bottom). (Right) Visual field coverage in Cartesian space of each surface node within the rCaS and eCaS across all participants.

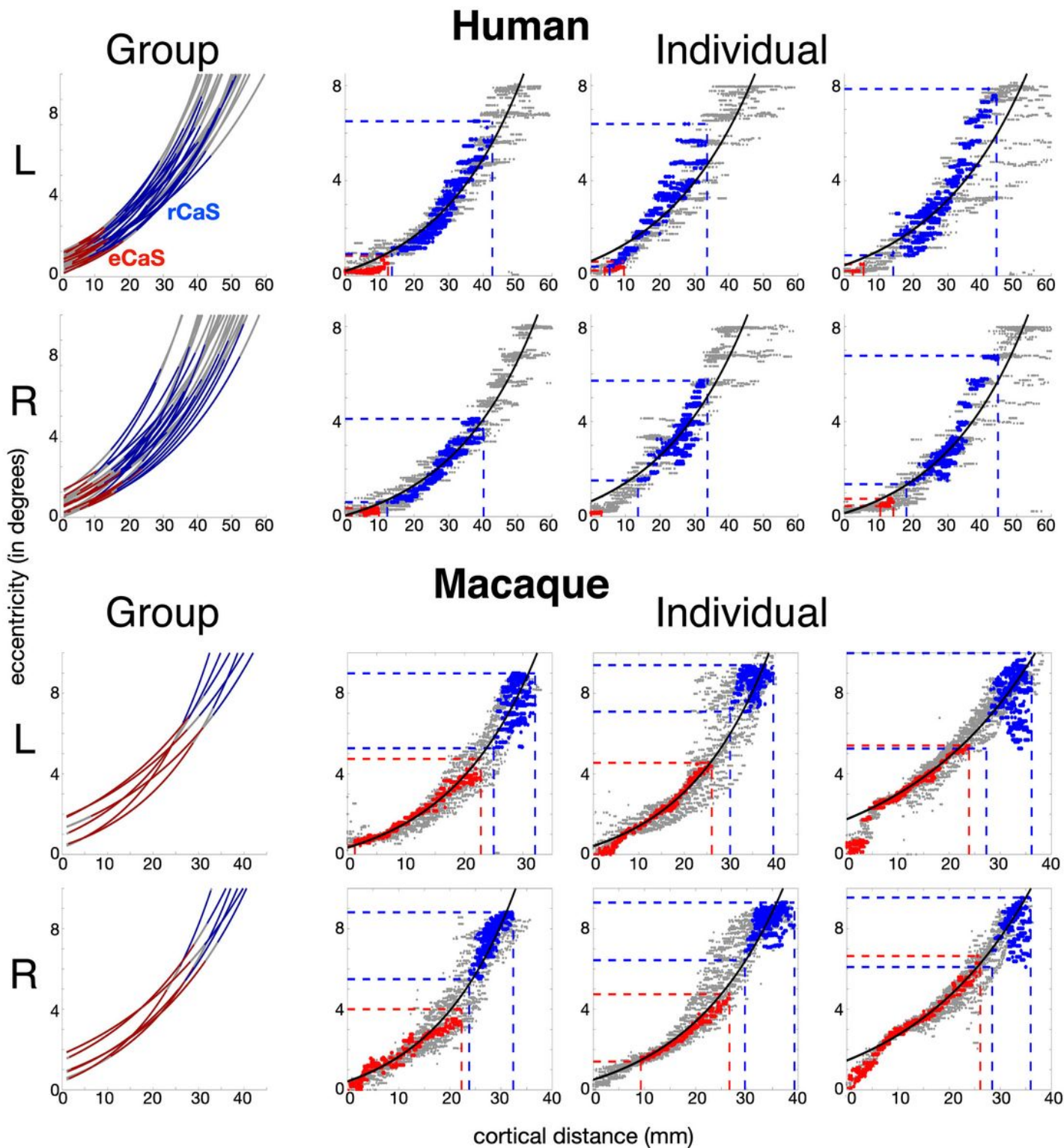


Figure 6

Eccentricity representations of rCaS and eCaS as a function of cortical distance in humans and macaques. (Left) Exponential curve fits to eccentricity as a function of cortical distance from V1's foveal confluence for each individual (Top) human and (Bottom) macaque. The range of eccentricity and cortical distances covered by the rCaS (blue line) and eCaS (red line) are shown relative to the rest of V1 (grey line). (Right) Scatter plots of eccentricity representations in relation to cortical distance from V1's fovea within the rCaS (blue), the eCaS (red), and the rest of V1 (grey) for three individuals. The range of eccentricity and cortical distances covered by the rCaS and eCaS are illustrated by red and blue dashed lines, respectively. See Supplementary Figure 4 for additional example individuals.

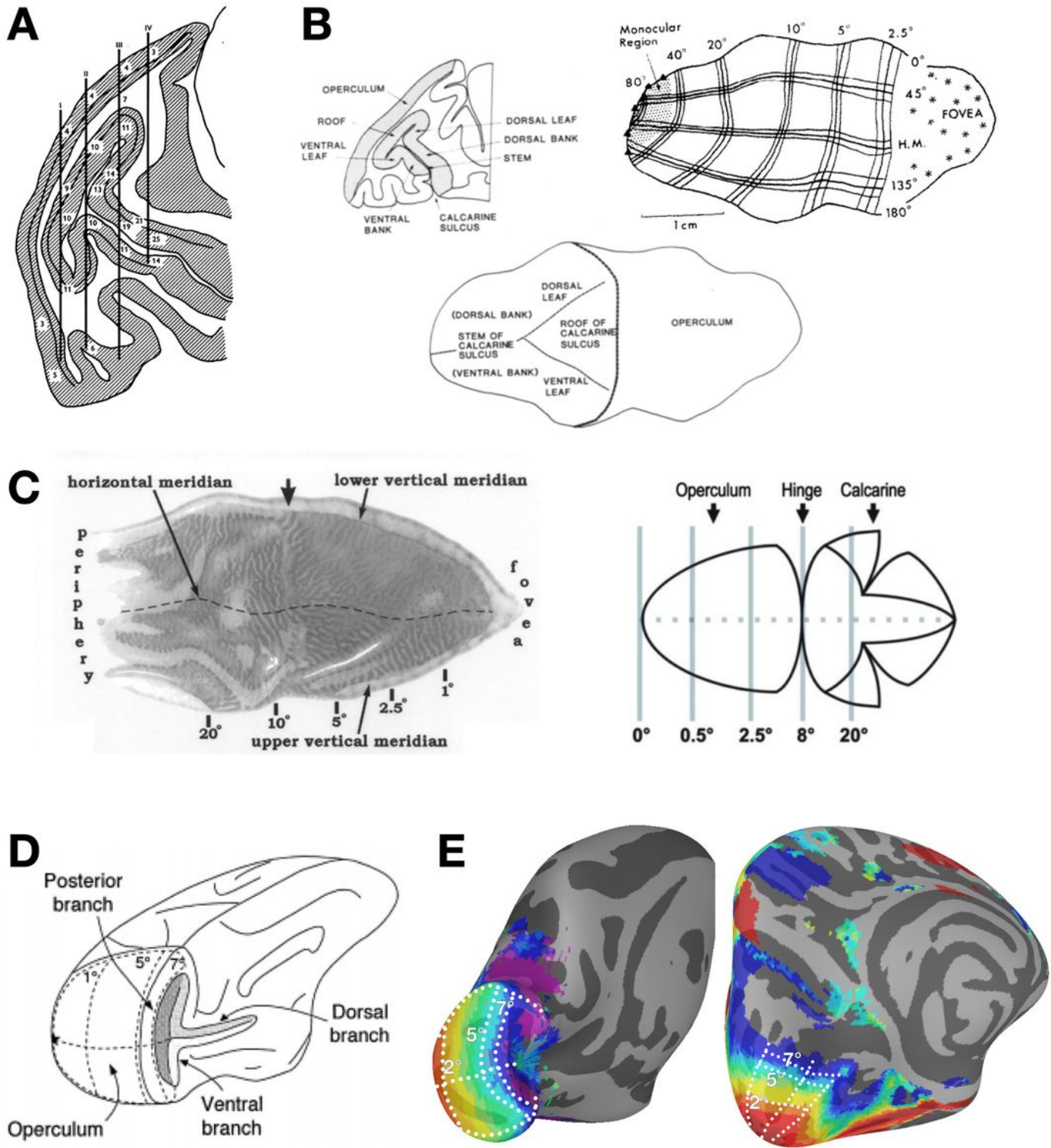


Figure 7

Eccentricity and the rCaS across species, methods, and time (1961-2021). (A) A drawing from Daniel and Whittredge (1961) of a baboon's brain. Needle tracks (vertical black lines) are depicted relative to cortical locations that reflect the preferred neuronal firing to spots of light at a particular radial distance from the fixation point (numbers). (B) Left: A drawing of a coronal slice from a macaque brain showing different parts of the rCaS (roof, ventral leaf, and dorsal leaf; Van Essen et al., 1984). Right, Bottom: Drawings of

flattened versions of V1 with labeled eccentricity values relative to the three pieces of the rCaS. Images adapted from Van Essen et al., 1984. (C) Left: A flattened version of V1 stained with cytochrome oxidase and labeled with eccentricity values, in which the arrow denotes 8°. Right: A schematic version of the leftmost image. Images adapted from Horton and Hocking, 1996. (D) A drawing of a macaque brain, slightly rotated and labeled with eccentricity values in which 7° is just posterior to the rCaS (labeled here as “posterior branch)” from Galletti et al., 2001. (E) Eccentricity maps on inflated cortical surfaces for (left) macaques and (right) humans from the present group average data.

Supplementary Files

This is a list of supplementary files associated with this preprint. Click to download.

- [RetrocalcarineSupplementaryFigurespenultimate.pdf](#)